metals

Article

Critical Conditions for Dynamic Recrystallization of S280 Ultra-High-Strength Stainless Steel Based on Work Hardening Rate

Mutong Liu [1,*], Ye Tian [1], Yu Wang [1], Kelu Wang [2], Kaiming Zhang [2] and Shiqiang Lu [2]

[1] AECC Beijing Institute of Aeronautical Materials, Beijing 100095, China; ye.tian@biam.ac.cn (Y.T.); yu.wang@biam.ac.cn (Y.W.)
[2] School of Aeronautical Manufacturing Engineering, Nanchang Hangkong University, Nanchang 330063, China; 29018@nchu.edu.cn (K.W.); 2003085600108@stu.nchu.edu.cn (K.Z.); niatlusq@nchu.edu.cn (S.L.)
* Correspondence: mutong.liu@biam.ac.cn; Tel.: +86-010-6249-7583

Abstract: Isothermal and constant-strain-rate compression experiments for S280 ultra-high-strength stainless steel were carried out under deformation temperatures of 1000–1150 °C and strain rates of 0.001–10 s^{-1} with a Thermecmaster-Z thermal simulator. The flow–stress behavior of the alloy was studied and the hot deformation activation energy was calculated. A critical strain model of the dynamic recrystallization (DRX) of the alloy was established using the work hardening rate for the first time. The results show that S280 ultra-high-strength stainless steel was positively sensitive to the strain rate and negatively sensitive to temperature, and its flow–stress curve showed characteristics of flow softening. The hot deformation activation energy corresponding to the peak strain was 519.064 kJ/mol. The DRX critical strain of the steel was determined from the minimum value of the $-\partial(\ln\theta)/\partial\varepsilon - \varepsilon$ curve. The relationship between the DRX critical strain and peak strain could be characterized as $\varepsilon_c = 0.599\varepsilon_p$ and the relationship between the DRX critical stress and peak stress could be characterized as $\sigma_c = 0.959\sigma_p$ The critical strain model of DRX could be expressed as $\varepsilon_c = 0.010Z^{0.062}$. The research results can provide theoretical support for avoiding the generation of actual thermal processing microstructure defects such as coarse grains and for obtaining products with excellent microstructure and properties.

Keywords: S280 ultra-high-strength stainless steel; flow stress; work hardening rate; dynamic recrystallization critical strain model

Citation: Liu, M.; Tian, Y.; Wang, Y.; Wang, K.; Zhang, K.; Lu, S. Critical Conditions for Dynamic Recrystallization of S280 Ultra-High-Strength Stainless Steel Based on Work Hardening Rate. *Metals* **2022**, *12*, 1123. https://doi.org/10.3390/met12071123

Academic Editors: Minghui Cai, Shuai Tang and Shengjie Yao

Received: 4 June 2022
Accepted: 28 June 2022
Published: 30 June 2022

1. Introduction

S280 ultra-high-strength stainless steel is a new type of structural material. It has excellent overall properties such as ultra-high strength, high toughness, excellent corrosion resistance and good fatigue resistance [1]. S280 steel is mainly used in marine applications, aviation and the manufacture of other equipment, such as ship shells, aircraft landing gear, wing beams and fasteners. It is an important metal for main-bearing and corrosion-resistant components [2,3]. The current research on S280 steel mainly focuses on the influence of heat-treatment parameters on the microstructure, mechanical properties and pitting corrosion behavior. Zhong et al. [4] studied the microstructure of S280 steel and found a new precipitation phase, Cr_2C, in addition to Fe_2Mo, and its crystallographic orientation relationship with martensite was also determined. Zhong et al. [5] studied the effect of the solution and aging temperatures on the microstructure and properties of S280 steel and found that S280 steel had the best mechanical properties with a 1080 °C solution temperature and 560 °C aging temperature. Zhan et al. [6] studied the passivation process for S280 steel, obtained the best passivation process parameters and found that the corrosion resistance after passivation was significantly improved, while the fatigue resistance was only slightly lower. Zhong et al. [7] studied the passivation breakdown resistance and pitting corrosion behavior of S280 steel and 300M steel in a borate solution containing chloride ions, and found that S280 steel showed shallower pitting corrosion and stronger breakdown resistance than 300M steel. Tian et al. [8] studied the shot peening process for S280 steel; the fatigue life of the steel was significantly improved after shot peening. However, there are few reports on the dynamic recrystallization behavior of S280 ultra-high-strength stainless steel during hot deformation.

Dynamic recrystallization (DRX) is one of the most important softening mechanisms for materials in thermal deformation, as it can refine the grains, produce the required microstructure and improve the mechanical properties as desired [9]. The critical conditions for DRX are the corresponding strain and stress at the initiation of DRX, which is closely related to the thermal-deformation conditions. The critical conditions for DRX under various thermal-processing parameters should be determined, and a corresponding critical strain model, which has important guiding significance for judging whether DRX occurs in the process of thermal deformation, should be established [10]. The critical conditions for DRX are mostly determined from the work hardening rate ($\theta = d\sigma/d\varepsilon$) proposed by Poliak and Jonas [11]. This has been successfully applied for steel [12], magnesium alloys [13], aluminum alloys [14], titanium alloys [15] and other materials, showing good applicability and relatively high precision. The method involves processing flow–stress curve data based on the work hardening rate (θ) to reflect the dynamic recrystallization softening characteristics of the material during thermal deformation; that is, an inflection point appears on the $\theta - \sigma$ (or $\ln\theta - \varepsilon$) curve when dynamic recrystallization occurs and the $-\partial\theta/\partial\sigma - \sigma$ (or $-\partial(\ln\theta)/\partial\varepsilon - \varepsilon$) curve has a minimum value [16,17]. The critical strain of DRX can be determined from the inflection point and minimum value on the corresponding strain curve.

In this work, the flow–stress behavior of S280 ultra-high-strength stainless steel was studied under deformation temperatures of 1000–1150 °C and strain rates of 0.001–10 s^{-1}. The hot deformation activation energy was calculated. The critical conditions for DRX were determined from the work hardening rate and a strain model for DRX was established.

2. Materials and Methods

The S280 steel employed in the present work was provided in the form of a forged bar with a diameter of 180 mm. The chemical composition of the S280 steel bar was 0.10C-12.3Cr-13.2Co-4.6Mo-3.0Ni-0.9W-0.16V-balance Fe, wt.%. The original microstructure of the S280 steel is shown in Figure 1. Before the experiment, the compression specimens, with a diameter of 8 mm and length of 12 mm, were machined with their cylinder axes parallel to the axial line direction of the bar. Isothermal constant-strain-rate compression experiments were conducted on a Thermecmaster-Z thermal–mechanical simulator (Fuji Kiko Co., Ltd., Shizuoka, Japan). The specimens were heated at a rate of 5 °C/s and held at a certain temperature for 300 s to ensure a uniform starting temperature and decrease the material anisotropy. All the specimens were compressed to realize a height reduction of 70% at temperatures of 1000, 1050, 1100 and 1150 °C, and strain rates of 0.001, 0.01, 0.1, 1 and 10 s^{-1}; then, they were immediately cooled with argon (50 °C/s) to retain the recrystallized microstructures. The compressed specimens were cut, polished, electrolytically corroded and then photographed using an XJP-9A metallographic microscope (Omu Micro Technology Co., Ltd., Shenzen, China) to obtain the microstructure after compression.

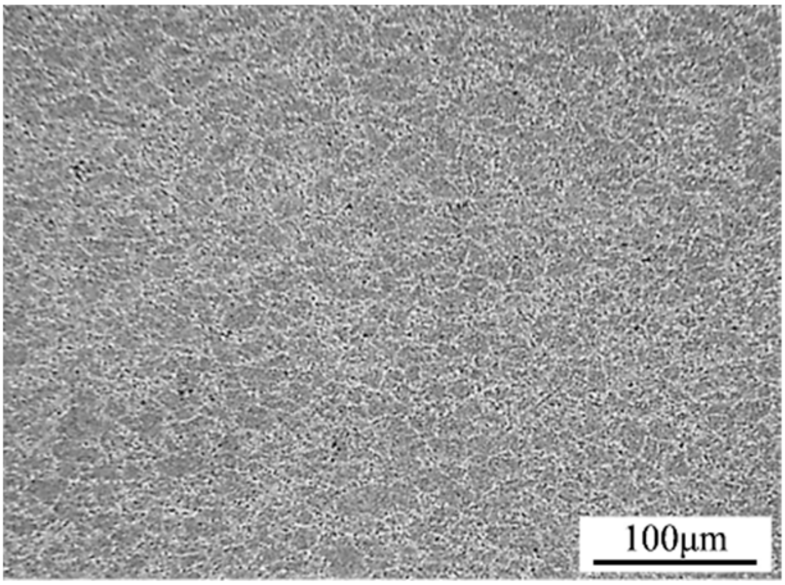

Figure 1. Original microstructure of S280 ultra-high-strength stainless steel.

3. Results

3.1. Analysis of Flow-Stress Curves

The flow–stress curves of the S280 ultra-high-strength stainless steel under different deformation conditions are illustrated in Figure 2. It can be seen that the flow stress of the S280 steel increased with an increase in the strain rate and decreased with the deformation temperature, indicating that the S280 steel was positively sensitive to the strain rate and negatively sensitive to the temperature. In the initial stage of deformation, the flow stress increased sharply with an increase in strain. This was due to the rapid increase in dislocation density in the material due to deformation, and the work hardening effect of the deformation played a leading role. The dynamic recovery caused by dislocation climbing and slip cannot easily counteract the hardening effect, resulting in an increase in flow stress [18,19]. With a further increase in the deformation, the flow stress increased to the peak stress and then decreased gradually, showing the characteristics of flow softening. This was due to the continuous increase in the strain, exceeding the critical strain of DRX, and DRX increased the dynamic softening effect. After the peak stress, the effect of dynamic softening began to dominate and the flow stress gradually decreased. Finally, most of the flow–stress curves tended to stabilize after the strain reached 0.8, at which point the effects of work hardening and dynamic softening reached an equilibrium [20,21]. In Figure 2a–c, many obvious multi-peak shapes appear many times on the flow–stress curves for a strain rate of 1 s^{-1}, indicating that the material underwent discontinuous DRX at this strain rate; that is, during the deformation process, the softening and hardening effects alternated many times [22]. From Figure 2d, it can be seen that, when the strain was greater than about 0.7, all the curves were upturned. This may be because the lubricating conditions deteriorated at the high temperature of 1150 °C, the frictional stress on the end face of the specimen increased, and the actual stress state changed from a one-way to three-way state, resulting in an increase in flow stress [23,24]. In addition, with the progress of thermal compression, the contact area between the indenter and the specimen increased and the influence of the end-face friction on the flow stress increased, resulting in an obvious upturn in the flow–stress curve when the strain was greater than about 0.7.

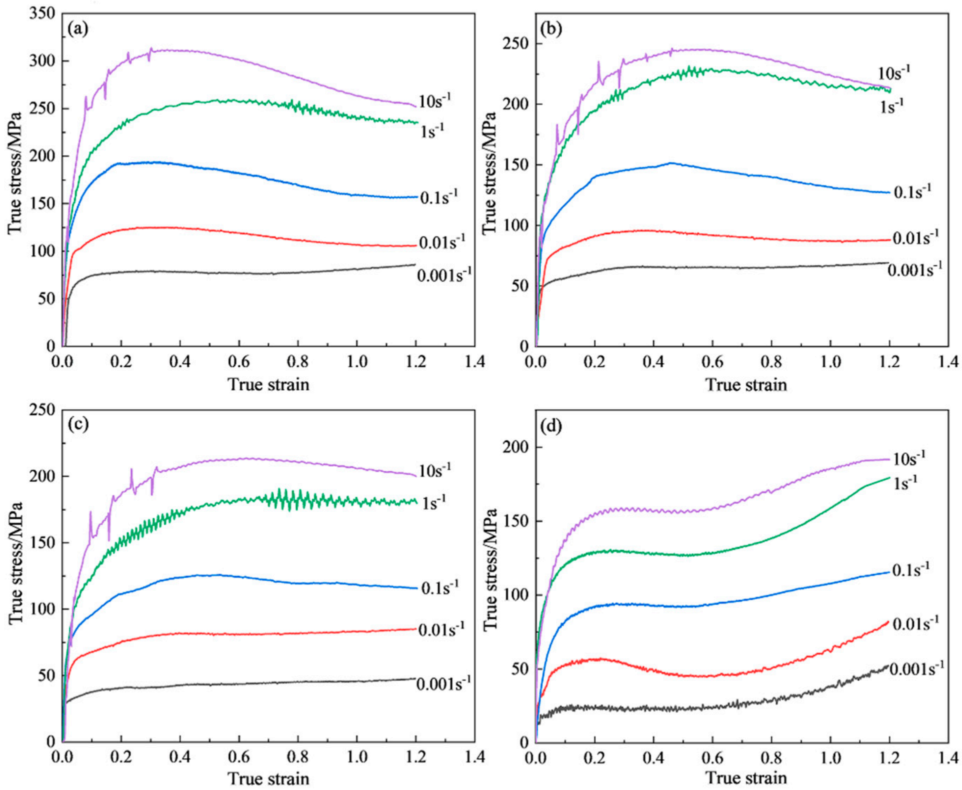

Figure 2. Flow-stress curves under different deformation conditions. (**a**) 1000 °C; (**b**) 1050 °C; (**c**) 1100 °C; (**d**) 1150 °C.

3.2. Calculation of Thermal-Deformation Activation Energy

The thermal-deformation activation energy is an important material parameter that characterizes the difficulty of plastic deformation at high temperature, and is closely related to multiple processes of thermal deformation [25,26]. The thermal-deformation activation energy of S280 steel can be calculated according to the Arrhenius equation, and its expressions are as follows [27,28]:

$$\dot{\varepsilon} = A_1 \sigma^{n_1} \exp\left(-\frac{Q}{RT}\right), \quad \alpha\sigma < 0.8 \tag{1}$$

$$\dot{\varepsilon} = A_2 \exp(\beta\sigma) \exp\left(-\frac{Q}{RT}\right), \ \alpha\sigma > 1.2 \tag{2}$$

$$\dot{\varepsilon} = A_3 [\sin(\alpha\sigma)]^n \exp\left(-\frac{Q}{RT}\right), \text{ for all} \tag{3}$$

where $\dot{\varepsilon}$ is the strain rate (s^{-1}); σ is the flow stress (MPa) for a given strain; Q is the activation energy (kJ/mol); R is the universal gas constant (8.31 J/(mol·K)); T is the absolute temperature (K); A_1, A_2, A_3, n_1, n, α and β are all constants related to materials; and $\alpha = \beta/n_1$.

Taking the natural logarithms of Equations (1)–(3) yields the following expressions:

$$\ln \dot{\varepsilon} = \ln A_1 + n_1 \ln \sigma - (\frac{Q}{RT}) \tag{4}$$

$$\ln \dot{\varepsilon} = \ln A_2 + \beta\sigma - (\frac{Q}{RT}) \tag{5}$$

$$\ln \dot{\varepsilon} = \ln A_3 + n \ln[\sinh(\alpha\sigma)] - (\frac{Q}{RT}) \tag{6}$$

The thermal-deformation activation energy, Q, can be expressed as:

$$Q = R \cdot \left[\frac{\partial \ln[\sin h(\alpha\sigma)]}{\partial\left(\frac{1}{T}\right)} \right] \cdot \left[\frac{\partial \ln \dot{\varepsilon}}{\partial \ln[\sin h(\alpha\sigma)]} \right] = Rkn \tag{7}$$

According to the isothermal constant-strain-rate compression experimental data, the peak stress (σ_p) of the S280 steel under different deformation conditions could be determined. Then, $\ln \dot{\varepsilon} - \ln\sigma_p$ and $\ln\dot{\varepsilon} - \sigma_p$ fitting curves could be drawn from Equations (4) and (5), as shown in Figure 3. The average value of the slope of the fitted straight line is represented by the parameters n_1 and β. The value of parameter α can be obtained according to the relationship $\alpha = \beta/n_1$. From Equations (6) and (7) and the obtained α value, the fitting curves of $\ln[\sin h(\alpha\sigma_p)] - 1/T$ and $\ln\dot{\varepsilon} - \ln[\sin h(\alpha\sigma_p)]$ can be obtained, as shown in Figure 4, whereas the average value of the slope of the fitted line is represented by the parameters k and n. In summary, the values of the parameters n_1, β, α, n and k are 5.671, 0.054, 0.009, 4.088 and 15,270.62, respectively. After substituting the relevant parameters into Equation (7), the thermal-deformation activation energy could be calculated to be 519.064 kJ/mol.

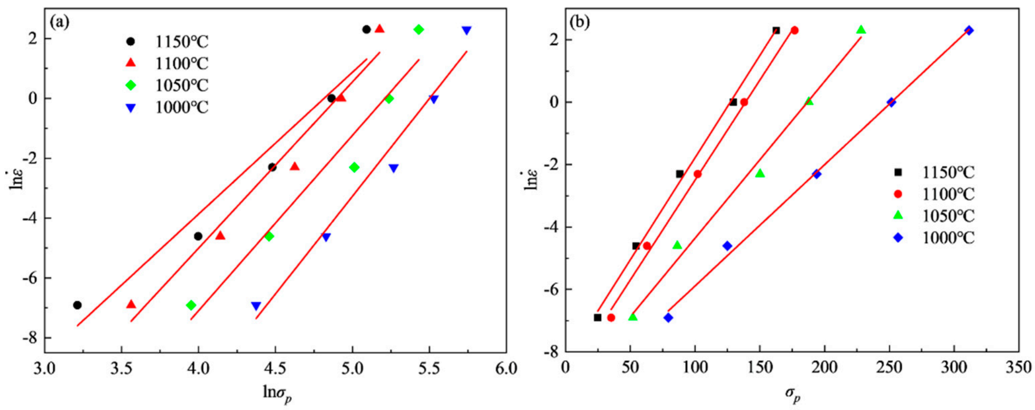

Figure 3. $\ln \dot{\varepsilon} - \ln\sigma_p$ and $\ln\dot{\varepsilon} - \sigma_p$ fitting curves for S280 steel at different deformation temperatures: (**a**) $\ln \dot{\varepsilon} - \ln\sigma_p$; (**b**) $\ln\dot{\varepsilon} - \sigma_p$.

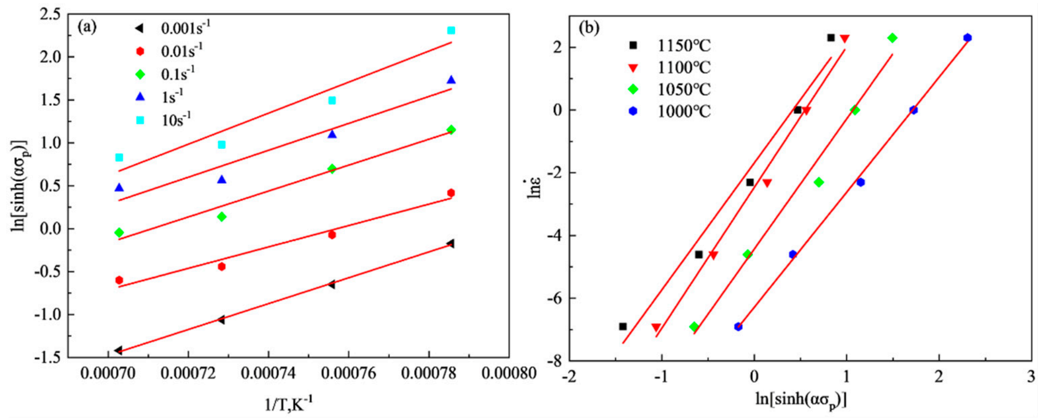

Figure 4. $\ln[\sin h(\alpha\sigma_p)] - 1/\mathrm{T}$ and $\ln\dot{\varepsilon} - \ln[\sin h(\alpha\sigma_p)]$ fitting curves for S280 steel: (**a**) $\ln[\sinh(\alpha\sigma_p)] - 1/\mathrm{T}$; (**b**) $\ln\dot{\varepsilon} - \ln[\sin h(\alpha\sigma_p)]$.

It is generally believed that, when the activation energy of the thermal deformation of metals is close to the activation energy of self-diffusion, the softening mechanism is dominated by dynamic recovery; when the activation energy of thermal deformation is much higher than the activation energy of self-diffusion, the softening mechanism is dominated by dynamic recrystallization [29]. During the dynamic recovery process, the migration of vacancies in the material and the rearrangement and annihilation of dislocations are realized by the diffusion mechanism, so the activation energy of thermal deformation is similar to that of self-diffusion. During the process of dynamic recrystallization, the nucleation and growth of dynamic recrystallization grains require more energy and the activation energy of thermal deformation is much higher than that of self-diffusion [25,30]. The calculated thermal deformation activation energy of S280 steel (519.064 kJ/mol) is much higher than the self-diffusion activation energy of γ-Fe (270 kJ/mol) [31] and also higher than that of the comparable steel A100 at peak strain (380.177 kJ/mol) [32], indicating that its main softening mechanism during thermal deformation is dynamic recrystallization. It can be seen from Figure 5 that, in addition to the coarse original grains, there are many fine DRX grains in the microstructure, which indicates that DRX occurs during hot deformation. The flow softening characteristics shown in the flow-stress curves in Figure 5 and high thermal-deformation activation energy, Q, are further proof that DRX occurs.

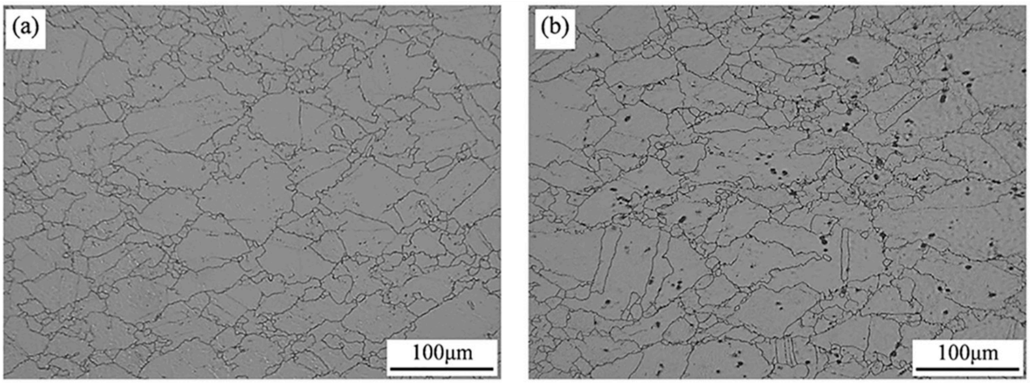

Figure 5. Microstructure of S280 steel at different deformation temperatures when the strain rate was 0.01 s^{-1} and the strain was 0.22: (**a**) 1100 °C; (**b**) 1150 °C.

3.3. *Identification of Critical Conditions for DRX*

3.3.1. Determination of Critical Strain for DRX Based on Work Hardening Rate

The work hardening rate (θ = dσ/dε) of a material is the rate at which the flow stress changes with strain. Generally, the flow-stress curve obtained in a hot compression experiment is not smooth (see Figure 2), and it is difficult to directly determine the slope (work hardening rate) corresponding to each point on the curve. It is necessary to perform high-precision fitting of the flow-stress curve to obtain the fitting equation. Through the derivation of the equation, the work hardening rate at each strain can be obtained. By drawing the $\ln\theta - \varepsilon$ curve and the $-\partial(\ln\theta)/\partial\varepsilon - \varepsilon$ curve, the critical strain and stress values for DRX can be determined according to the inflection point on the $\ln\theta - \varepsilon$ curve and the minimum value on the $-\partial(\ln\theta)/\partial\varepsilon - \varepsilon$ curve.

Taking the flow-stress curve of the S280 steel under the conditions of a deformation temperature of 1150 °C and strain rate of 1 s^{-1} as an example, the specific steps of the method are described below. First, the flow-stress curve was fitted, as shown in Figure 6; the correlation coefficient, R, was 0.999, and the corresponding fitting equation is:

$$\sigma = p_1 + p_2\varepsilon^{0.5} + p_3\varepsilon + p_4\varepsilon^{1.5} + p_5\varepsilon^2 + p_6\varepsilon^{2.5} + p_7\varepsilon^3 + p_8\varepsilon^{3.5} + p_9\varepsilon^4 \quad (8)$$

where σ is the flow stress (MPa), ε is the strain, and $p_1 - p_9$ are coefficients; their values are shown in Table 1.

Secondly, through the derivation of Equation (8), the work hardening rate under this deformation condition can be calculated and the $\ln\theta - \varepsilon$ curve can be further drawn, as shown in Figure 7a. Then, cubic fitting was performed on the $\ln\theta - \varepsilon$ curve in Figure 7a and the result was:

$$\ln\theta = 8.92110 - 86.88992\varepsilon + 669.25928\varepsilon^2 - 1890.544\varepsilon^3 \quad (9)$$

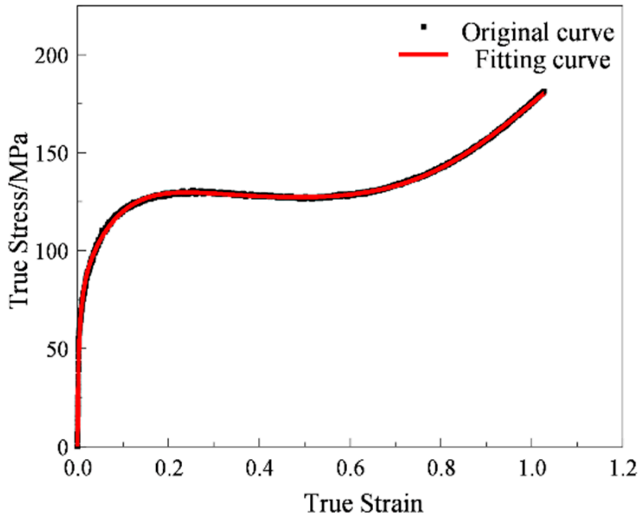

Figure 6. Original and fitting curves for flow-stress of S280 steel at a deformation temperature of 1150 °C and strain rate of 1 s^{-1}.

Table 1. Flow-stress fitting curve equation coefficients for S280 steel at a deformation temperature of 1150 °C and strain rate of 1 s^{-1}.

p_1	p_2	p_3	p_4	p_5
−8.56726	1584.41009	−11,783.86258	55,897.71989	−158,546.47991
p_6	p_7	p_8	p_9	
268,037.44580	−265,828.82359	142,943.98934	−32,120.70831	

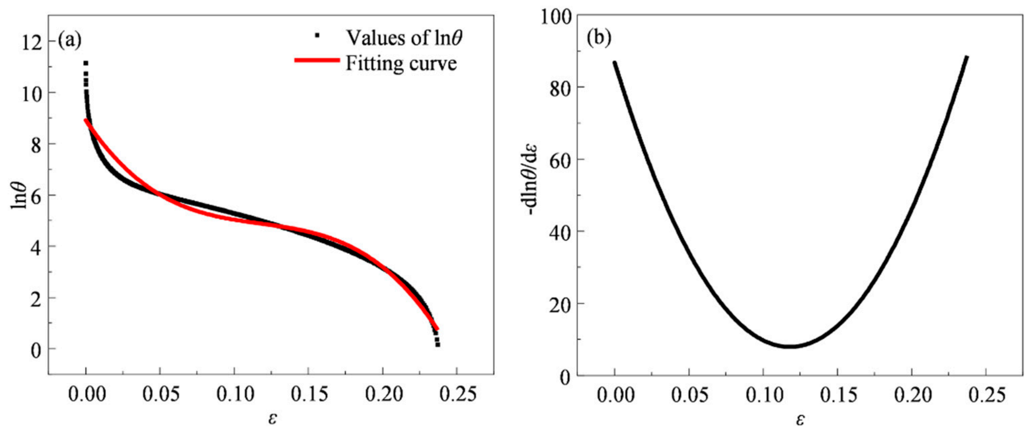

Figure 7. Relationship between $\ln\theta - \varepsilon$ and $-\partial(\ln\theta)/\partial - \varepsilon$ for S280 steel at a deformation temperature of 1150 °C and strain rate of 1 s^{-1}: (**a**) $\ln\theta - \varepsilon$; (**b**) $-\partial(\ln\theta)/\partial\varepsilon - \varepsilon$.

Taking the derivative of this equation yielded the following expression:

$$\frac{\partial(\ln\theta)}{\partial\varepsilon} = \frac{-35447700\varepsilon^2 + 8365741\varepsilon - 543062}{6250} \tag{10}$$

According to Equation (10), the $-\partial(\ln\theta)/\partial\varepsilon - \varepsilon$ curve is as shown in Figure 7b. The minimum value (corresponding to the inflection point on the $\ln\theta - \varepsilon$ curve) is the critical strain for DRX under this deformation condition, and its value is 0.1179.

Figure 8 shows the microstructure of the S280 steel under different strains at a deformation temperature of 1150 °C and strain rate of 1 s^{-1}. It can be seen from Figure 8a that, when the S280 steel was heated to 1150 °C without deformation, its grains were equiaxed and uniform in size, and the grain boundaries were relatively straight. When it was deformed with a strain of 0.11 at 1150 °C, as shown in Figure 8b, a small amount of DRX grains could be clearly observed at the trigeminal grain boundary and the DRX volume fraction was about 5.2%, indicating that DRX occurred. When the s train increased to 0.43, as shown in Figure 8c, a large number of DRX grains appeared in the steel, and the DRX volume fraction reached about 64.6%. When the strain was increased to 1.2, the ultra-high-strength stainless steel underwent complete DRX and the grains were also significantly refined. The above microstructural observations may confirm that the DRX critical strain for S280 steel at 1150 °C and a strain rate of 1 s^{-1} is about 0.11, which is similar to the result determined from the work hardening rate. This shows that the work-hardening-rate method has high accuracy for determining the critical strain for DRX during the thermal deformation of S280 ultra-high-strength stainless steel.

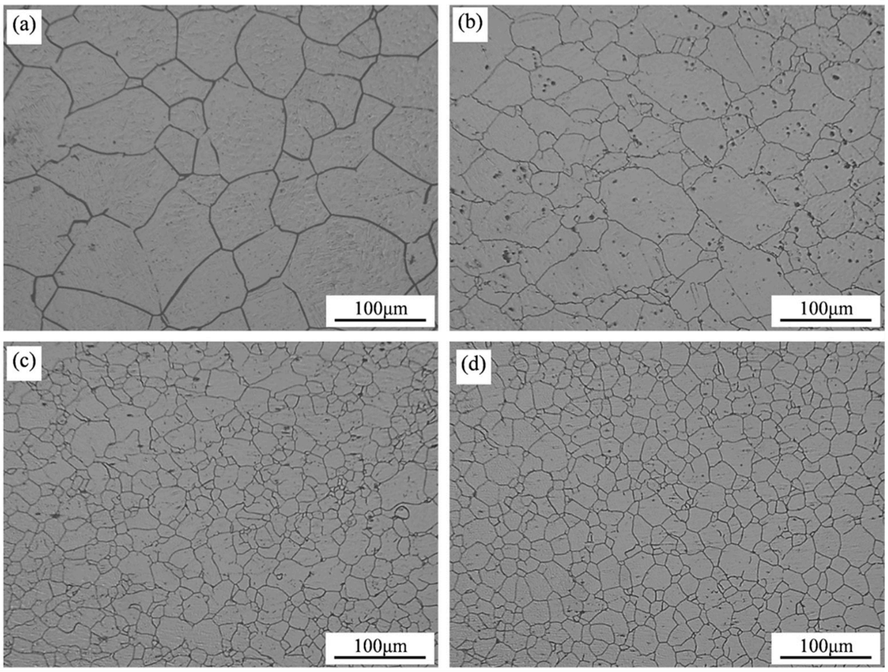

Figure 8. Microstructure of S280 steel under different strains at a deformation temperature of 1150 °C and strain rate of 1 s^{-1}: (**a**) $\varepsilon = 0$; (**b**) $\varepsilon = 0.11$; (**c**) $\varepsilon = 0.43$; (**d**) $\varepsilon = 1.2$.

Therefore, according to the above method, the work hardening rate of S280 steel under other deformation conditions can be obtained and the relationship curves of $\ln\theta - \varepsilon$ and $-\partial(\ln\theta)/\partial\varepsilon - \varepsilon$ can be drawn, as shown in Figures 9–13. The critical strain for DRX under various deformation conditions could be determined from Figures 9–13 and the results are shown in Table 2. The critical stress for DRX was obtained from the critical strain and the results are shown in Table 3. It can be seen from Tables 2 and 3 that, under the experimental conditions of the present work, the critical strain was approximately in the range of 0.0647–0.1907, and the critical stress was approximately in the range of 19.5478–294.9036 MPa.

3.3.2. Identification of DRX Critical Strain Model

As an important parameter for characterizing DRX, the critical strain for DRX is the key to studying the behavior of DRX. Therefore, it was necessary to establish a critical strain model for DRX during the hot deformation of S280 steel. The widely used Sellars model was used to establish the DRX critical strain model for the ultra-high-strength stainless steel [33]; its expressions are as follows:

$$\varepsilon_c = a\varepsilon_p \tag{11}$$

$$\varepsilon_p = a_1 Z^{a_2} \tag{12}$$

$$Z = \dot{\varepsilon} \exp\left(\frac{Q}{RT}\right) \quad (13)$$

where ε_c is the critical strain for DRX; ε_p is the peak strain; a, a_1 and a_2 are constants; Z is the Zener-Hollomon parameter, that is, the strain rate factor of temperature compensation; and Q is the activation energy of thermal deformation, with a value of 519.064 kJ/mol.

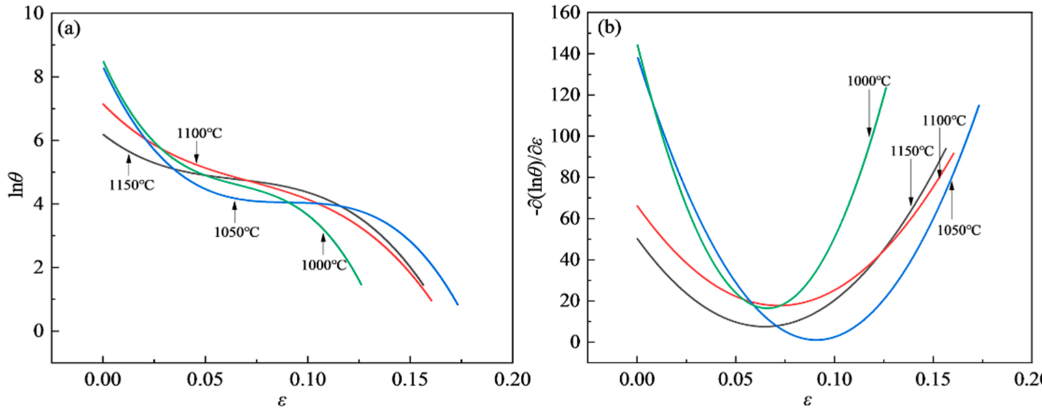

Figure 9. Relationship between $\ln\theta - \varepsilon$ and $-\partial(\ln\theta)/\partial\varepsilon - \varepsilon$ for S280 steel at a strain rate of 0.001 s^{-1} and different deformation temperatures: (**a**) $\ln\theta - \varepsilon$; (**b**) $-\partial(\ln\theta)/\partial\varepsilon - \varepsilon$.

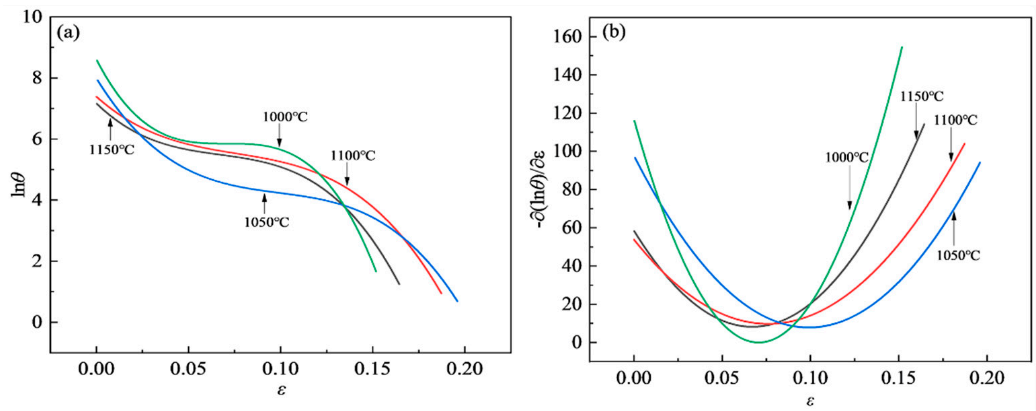

Figure 10. Relationship between $\ln\theta - \varepsilon$ and $-\partial(\ln\theta)/\partial\varepsilon - \varepsilon$ for S280 steel at a strain rate of 0.01 s^{-1} and different deformation temperatures: (**a**) $\ln\theta - \varepsilon$; (**b**) $-\partial(\ln\theta)/\partial\varepsilon - \varepsilon$.

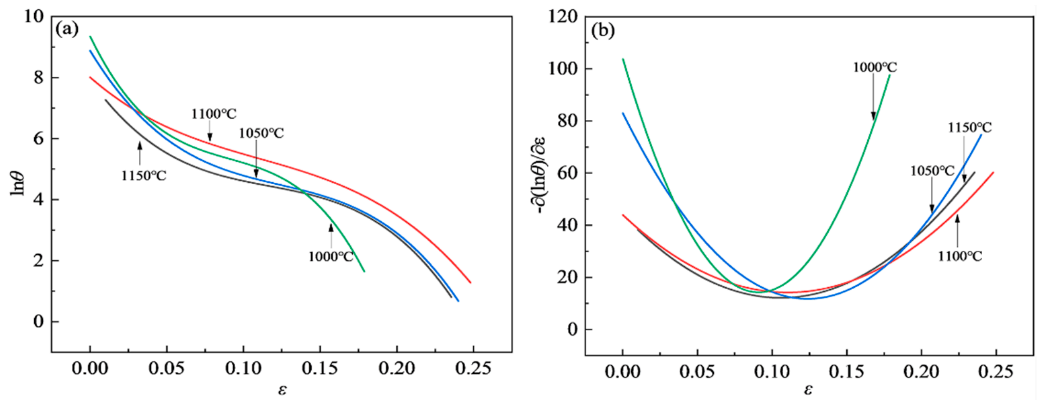

Figure 11. Relationship between $\ln\theta - \varepsilon$ and $-\partial(\ln\theta)/\partial\varepsilon - \varepsilon$ for S280 steel at a strain rate of 0.1 s^{-1} and different deformation temperatures: (**a**) $\ln\theta - \varepsilon$; (**b**) $-\partial(\ln\theta)/\partial\varepsilon - \varepsilon$.

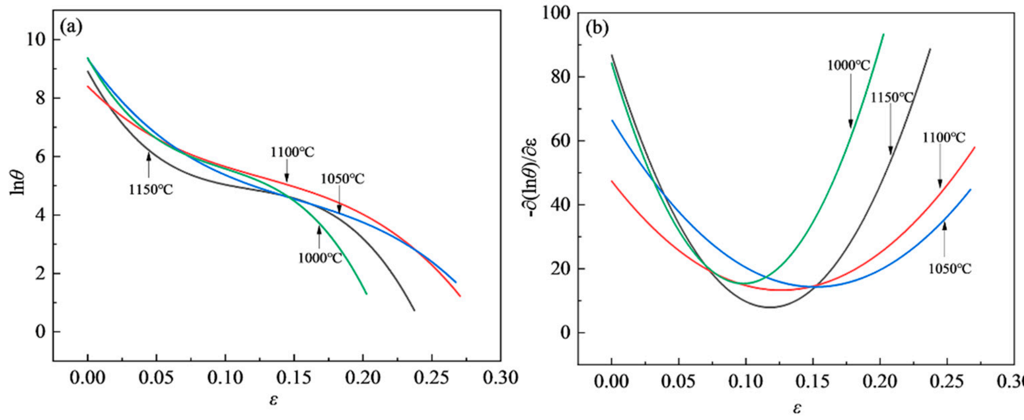

Figure 12. Relationship between $\ln\theta - \varepsilon$ and $-\partial(\ln\theta)/\partial\varepsilon - \varepsilon$ for S280 steel at a strain rate of 1 s^{-1} and different deformation temperatures: (**a**) $\ln\theta - \varepsilon$; (**b**) $-\partial(\ln\theta)/\partial\varepsilon - \varepsilon$.

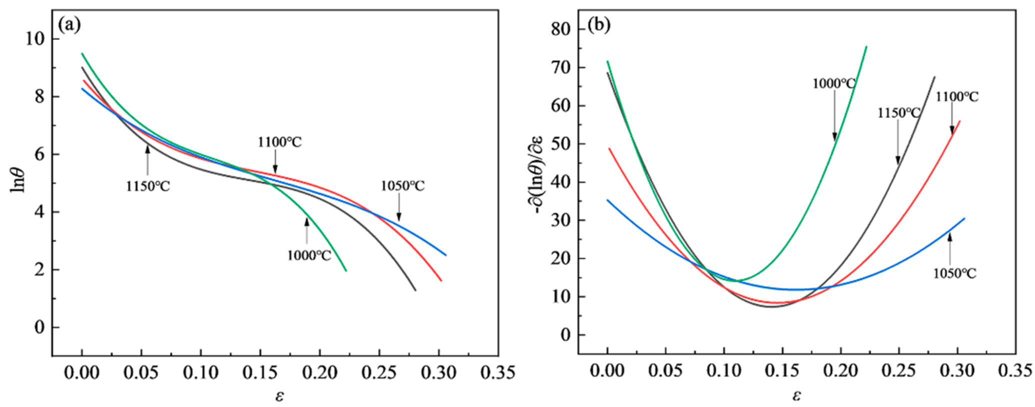

Figure 13. Relationship between $\ln\theta - \varepsilon$ and $-\partial(\ln\theta)/\partial\varepsilon - \varepsilon$ for S280 steel at a strain rate of 10 s^{-1} and different deformation temperatures: (**a**) $\ln\theta - \varepsilon$; (**b**) $-\partial(\ln\theta)/\partial\varepsilon - \varepsilon$.

Table 2. Dynamic recrystallization critical strain for S280 steel.

Strain Rate/s^{-1}	Deformation Temperature/°C			
	1000	**1050**	**1100**	**1150**
0.001	0.1219	0.0906	0.0717	0.0647
0.01	0.1317	0.0991	0.0759	0.0670
0.1	0.1459	0.1237	0.1107	0.1057
1	0.1903	0.1516	0.1262	0.1179
10	0.1907	0.1616	0.1455	0.1408

Table 3. Dynamic recrystallization critical stress for S280 steel.

Strain Rate/s^{-1}	Deformation Temperature/°C			
	1000	**1050**	**1100**	**1150**
0.001	75.8377	49.3479	31.4305	19.5478
0.01	116.8907	83.2727	51.1994	43.8961
0.1	183.5235	146.1575	92.1629	82.8419
1	230.7050	183.7780	128.1499	123.0821
10	294.9036	218.9624	163.0207	153.2359

According to the critical strain and stress values for DRX in Tables 2 and 3 and the peak strain and stress values obtained according to Figure 2, the relationship curves of $\varepsilon_c - \varepsilon_p$ and $\sigma_c - \sigma_p$ were drawn, as shown in Figure 14. It can be seen that the critical strain and peak strain and the critical stress and peak stress show a good linear relationship, which can be obtained by linear fitting: $\varepsilon_c = 0.599\varepsilon_p$ and $\sigma_c = 0.959\sigma_p$. Introduce the statistical Pearson correlation coefficient r and the average relative error $AARE$ to measure the linear correlation with the following expressions.

$$r = \frac{\sum_{i=1}^{N}(C_i - \overline{C})(P_i - \overline{P})}{\sqrt{\sum_{i=1}^{N}(C_i - \overline{C})^2 \sum_{i=1}^{N}(P_i - \overline{P})^2}} \tag{14}$$

$$AARE = \frac{1}{N}\sum_{i=1}^{N}\left|\frac{C_i - P_i}{C_i}\right| \times 100\% \tag{15}$$

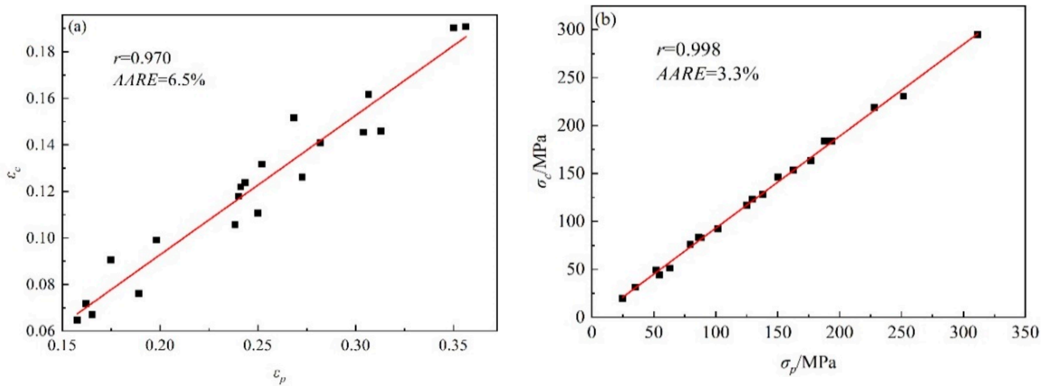

Figure 14. Relationship between $\varepsilon_c - \varepsilon_p$ and $\sigma_c - \sigma_p$ of S280 steel: (**a**) $\varepsilon_c - \varepsilon_p$; (**b**) $\sigma_c - \sigma_p$.

Taking the logarithm of Equation (12) yields the following expression:

$$\ln \varepsilon_p = lna_1 + a_2 \ln Z \tag{16}$$

The Z value and related parameters under each deformation condition calculated from Equation (13) were substituted into Equation (16), the lnε_p− ln$Z$ relationship curve was drawn and linear fitting (Figure 15) was performed. The calculations showed that a_1 = 0.016, a_2 = 0.062 and $\varepsilon_p = 0.016Z^{0.062}$.

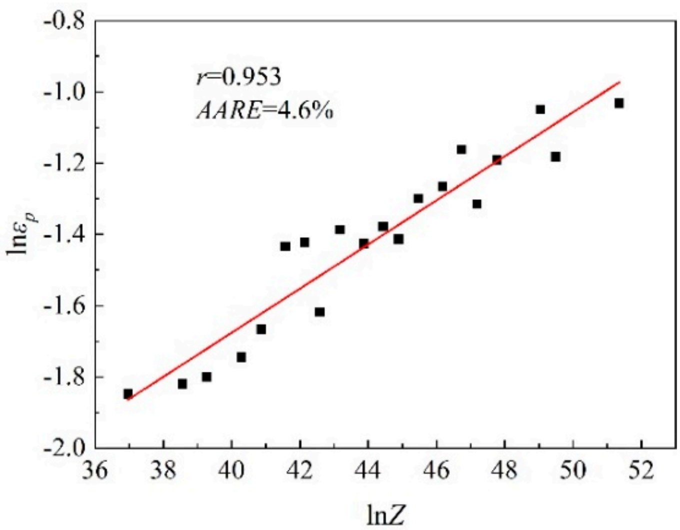

Figure 15. lnε_p − ln$Z$ linear relationship for S280 steel.

Based on the above results, the critical strain model for the DRX of S280 ultra-high-strength stainless steel is as follows:

$$\varepsilon_c = 0.010Z^{0.062} \quad (17)$$

4. Conclusions

- The flow stress of S280 ultra-high-strength stainless steel increases with an increase in strain rate and decreases with deformation temperature, and the flow–stress curve shows the characteristics of flow softening; the deformation activation energy between 1000 and 1150 °C is 519.064 kJ/mol. The flow softening and high deformation activation energy are caused by dynamic recrystallization during thermal deformation;
- Under the conditions of 1000–1150 °C and strain rates of 0.001–10 s^{-1}, the DRX critical strain for S280 steel determined based on the work-hardening-rate method is approximately 0.0647–0.1907, and the DRX critical stress is approximately 19.5478-294.9036 MPa;
- The relationship between the DRX critical strain and peak strain could be characterized as $\varepsilon_c = 0.599\varepsilon_p$ and the relationship between the DRX critical stress and peak stress could be characterized as $\sigma_c = 0.959\sigma_p$. The critical strain model for DRX could be expressed as $\varepsilon_c = 0.010Z^{0.062}$;
- This study is helpful to master the microstructure evolution behavior of S280 steel during hot deformation. It can provide theoretical support for further numerical simulation of the forming process and precise control of microstructure, allowing the creation of practical components with excellent microstructure and properties.

Author Contributions: Conceptualization, M.L.; methodology, K.W. and S.L.; formal analysis, Y.T.; investigation, Y.W.; data curation, M.L., K.W. and K.Z.; writing—original draft preparation, M.L.; writing—review and editing, K.W.; supervision, S.L.; funding acquisition, Y.T. All authors have read and agreed to the published version of the manuscript.

Funding: The research was funded by Key R&D Project of Aviation Key Materials China (No. 19-016).

Data Availability Statement: Data are contained within the article.

Conflicts of Interest: The authors declare no conflict of interest.

References

1. Zhong, P.; Zhang, Y.Q.; Zhong, J.Y.; Liu, M.T.; Xiao, K. A new type of structural material S280. *Sci. Technol. Rev.* **2015**, *33*, 59–62.
2. Liu, Z.B.; Liang, J.X.; Su, J.; Wang, X.H.; Sun, Y.Q.; Wang, C.J.; Yang, Z.Y. Research and application progress in ultra—High strength stainless steel. *Acta Metall. Sin.* **2020**, *56*, 549–557.
3. Niu, Y.E.; Zhao, P.P.; Li, N.; Song, J. Research status and application of ultra—High strength steel at home and abroad. *J. Ord. Eq. Eng.* **2021**, *42*, 274–279.
4. Zhong, J.Y.; Zhang, Y.Q.; Han, Y.F. New phase precipitated from the new type of ultrahigh strength stainless steel S280. *Rare Met. Mater. Eng.* **2019**, *48*, 116–122.
5. Zhong, J.Y.; Chen, Z.; Yang, S.L.; Li, S.M.; Liu, J.H.; Yu, M. Effect of solution and aging temperatures on microstructure and mechanical properties of 10Cr13Co13Mo5Ni3W1VE (S280) steel. *Micromachines* **2021**, *12*, 566. [CrossRef]
6. Zhan, Z.W.; Sun, Z.H.; Tang, Z.H. Effect of chemical passivation on properties of S280 ultra high—Strength stainless steel. *Corros. Prot.* **2015**, *36*, 742–758.
7. Zhong, J.Y.; Mao, F.X.; Ghanbari, E.; Macdonald, D.D. Passivity breakdown on 300 M and S280 ultra-high strength steels in borate buffer solutions containing chloride ion. *Electrochim. Acta* **2017**, *251*, 324–335. [CrossRef]
8. Tian, S.; Liu, P.G. Influence of shot peening on fatigue behavior of S280 ultrahigh strengh stainless steel. *J. Mater. Prot.* **2013**, *46*, 16–18.
9. Tian, Y.X.; Liu, C.; Cao, H.L.; Lin, H.T.; Wang, Z.A. Research progress of dynamic recrystallization in metallic materials. *Rare Met. Mater. Eng.* **2019**, *48*, 3764–3769.
10. Fang, B.; Ji, Z.; Liu, M.; Tian, G.F.; Jia, C.C.; Zeng, T.T.; Hu, B.F.; Chang, Y.H. Critical strain and models of dynamic recrystallization for FGH96 superalloy during two-pass hot deformation. *Mater. Sci. Eng. A* **2014**, *593*, 8–15. [CrossRef]
11. Poliak, E.I.; Jonas, J.J. A one-parameter approach to determining the critical conditions for the initiation of dynamic recrystallization. *Acta Mater.* **1996**, *44*, 127–136. [CrossRef]
12. Li, C.M.; Huang, L.; Zhao, M.J.; Zhang, X.T.; Li, J.J.; Li, P.C. Influence of hot deformation on dynamic recrystallization behavior of 300M steel: Rules and modeling. *Mater. Sci. Eng. A* **2020**, *797*, 139925. [CrossRef]

13. Wang, Z.T.; Liu, Y.Z.; Wang, M.H.; Liang, H.C. Study on dynamic recrystallization and grain size of magnesium alloy based on compound deformation. *J. Netshape Form. Eng.* **2021**, *13*, 115–120.
14. Li, D.Q.; Xu, L.; Huang, X.M.; Dai, G.Z. Investigation on gritical strain of dynamic recrystallization for 7A04 aluminum alloy. *J. Mater. Eng.* **2013**, *3*, 23–27.
15. Lin, X.J.; Huang, H.J.; Yuan, X.G.; Wang, Y.X.; Zheng, B.W.; Zuo, X.J.; Zhou, G. Study on high-temperature deformation mechanical behavior and dynamic recrystallization kinetics model of Ti-47.5 Al-2.5 V-1.0 Cr-0.2 Zr alloy. *J. Alloy. Compd.* **2022**, *891*, 162105. [CrossRef]
16. Ryan, N.D.; Mcqueen, H.J. Dynamic softening mechanisms in 304 austenitic stainless steel. *Can. Metall. Q.* **1990**, *29*, 147–162. [CrossRef]
17. Najafizadeh, A.; Jonas, J.J. Predicting the critical stress for initiation of dynamic recrystallization. *ISIJ Int.* **2006**, *46*, 1679–1684. [CrossRef]
18. Wang, R.; Zhang, W.; Li, Y.H.; Li, D.Z.; Kang, Y.; Yang, X.M.; Eckert, J.; Yan, Z.J. Stress-strain behavior and microstructural evolution of ultra-high carbon Fe-C-Cr-V-Mo steel subjected to hot deformation. *Mater. Charact.* **2021**, *171*, 110746. [CrossRef]
19. Wan, P.; Kang, T.; Li, F.; Gao, P.F.; Zhang, L.; Zhao, Z.Z. Dynamic recrystallization behavior and microstructure evolution of low-density high-strength Fe–Mn–Al–C steel. *J. Mater. Res. Technol.* **2021**, *15*, 1059–1068. [CrossRef]
20. Zhao, H.T.; Qi, J.J.; Su, R.; Zhang, H.Q.; Chen, H.W.; Bai, L.J.; Wang, C.M. Hot deformation behaviour of 40CrNi steel and evaluation of different processing map construction methods. *J. Mater. Res. Technol.* **2020**, *9*, 2856–2869. [CrossRef]
21. Mohammadi, H.; Eivani, A.R.; Seyedein, S.H.; Ghosh, M.; Jafarian, H.R. An investigation of hot deformation behavior of Zn–22Al alloy and development of its processing maps during isothermal compression. *J. Mater. Res. Technol.* **2021**, *14*, 507–520. [CrossRef]
22. Wang, X.K.; Xiao, D.H.; Wu, M.D.; Liu, W.S. Deformation behavior and microstructure evolution of Al–5.06 Mg–1.67 Li–0.51 Zn alloy under hot compression. *J. Mater. Res. Technol.* **2021**, *15*, 4516–4528. [CrossRef]
23. Zhai, Y.W.; Zhong, Z.P.; Jin, Q.L. Experimental research on mechanical property of P91 under high temperature thermal deformation. *J. Plast. Eng.* **2012**, *19*, 88–93.
24. Gao, W.L.; Guan, Y.F. Correction of flow stress−strain curve and processing maps of 5083 aluminum alloy during hot compression. *CHN J. Nonferrous Met.* **2018**, *28*, 1737–1745.
25. Sun, Y.; Wan, Z.P.; Hu, L.X.; Ren, J.S. Characterization of hot processing parameters of powder metallurgy TiAl-based alloy based on the activation energy map and processing map. *Mater. Des.* **2015**, *86*, 922–932. [CrossRef]
26. Long, J.C.; Xia, Q.X.; Xiao, G.F.; Qin, Y.; Yuan, S. Flow characterization of magnesium alloy ZK61 during hot deformation with improved constitutive equations and using activation energy maps. *Int. J. Mech. Sci.* **2021**, *191*, 106069. [CrossRef]
27. Sellars, C.M.; Mctegart, W.J. On the mechanism of hot deformation. *Acta Metall.* **1966**, *14*, 1136–1138. [CrossRef]
28. Lu, C.Y.; Wang, J.; Zhang, P.Z. Flow behavior analysis and flow stress modeling of Ti17 alloy in β forging process. *J. Mater. Eng. Perform.* **2021**, *30*, 7668–7681. [CrossRef]
29. Ryan, N.D.; Mcqueen, H.J. Comparison of dynamic softening in 301, 304, 316 and 317 stainless steels. *High Tem. Technol.* **1990**, *8*, 185–200. [CrossRef]
30. Wan, P.; Zou, H.; Wang, K.L.; Zhao, Z.Z. Hot deformation characterization of Ti–Nb alloy based on GA-LSSVM and 3D processing map. *J. Mater. Res. Technol.* **2021**, *13*, 1083–1097. [CrossRef]
31. Atkins, A.G. Deformation-mechanism maps (the plasticity and creep of metals and ceramics). *J. Mech. W Technol.* **1984**, *9*, 224–225. [CrossRef]
32. Ren, S.J. *Research on Isothermal Compression Behavior and Optimization of Process Parameters for A100 Ultra-High Strength Steel*; Nanchang Hangkong University: Nanchang, China, 2018.
33. Liu, X.G.; Zhang, L.G.; Qi, R.S.; Chen, L.; Jin, M.; Guo, B.F. Prediction of critical conditions for dynamic recrystallization in 316LN austenitic steel. *J. Iron Steel Res. Int.* **2016**, *23*, 238–243. [CrossRef]